Measurement of exclusive *D* meson decays to **η** and **η′** final states and SU(3) amplitude analysis

M. Artuso,[1] S. Blusk,[1] S. Khalil,[1] J. Li,[1] R. Mountain,[1] S. Nisar,[1] K. Randrianarivony,[1] N. Sultana,[1] T. Skwarnicki,[1] S. Stone,[1] J. C. Wang,[1] L. M. Zhang,[1] G. Bonvicini,[2] D. Cinabro,[2] M. Dubrovin,[2] A. Lincoln,[2] P. Naik,[3] J. Rademacker,[3] D. M. Asner,[4] K. W. Edwards,[4] J. Reed,[4] R. A. Briere,[5] T. Ferguson,[5] G. Tatishvili,[5] H. Vogel,[5] M. E. Watkins,[5] J. L. Rosner,[6] J. P. Alexander,[7] D. G. Cassel,[7] J. E. Duboscq,[7] R. Ehrlich,[7] L. Fields,[7] L. Gibbons,[7] R. Gray,[7] S. W. Gray,[7] D. L. Hartill,[7] B. K. Heltsley,[7] D. Hertz,[7] J. M. Hunt,[7] J. Kandaswamy,[7] D. L. Kreinick,[7] V. E. Kuznetsov,[7] J. Ledoux,[7] H. Mahlke-Krüger,[7] D. Mohapatra,[7] P. U. E. Onyisi,[7] J. R. Patterson,[7] D. Peterson,[7] D. Riley,[7] A. Ryd,[7] A. J. Sadoff,[7] X. Shi,[7] S. Stroiney,[7] W. M. Sun,[7] T. Wilksen,[7] S. B. Athar,[8] R. Patel,[8] J. Yelton,[8] P. Rubin,[9] B. I. Eisenstein,[10] I. Karliner,[10] S. Mehrabyan,[10] N. Lowrey,[10] M. Selen,[10] E. J. White,[10] J. Wiss,[10] R. E. Mitchell,[11] M. R. Shepherd,[11] D. Besson,[12] T. K. Pedlar,[13] D. Cronin-Hennessy,[14] K. Y. Gao,[14] J. Hietala,[14] Y. Kubota,[14] T. Klein,[14] B. W. Lang,[14] R. Poling,[14] A. W. Scott,[14] P. Zweber,[14] S. Dobbs,[15] Z. Metreveli,[15] K. K. Seth,[15] A. Tomaradze,[15] J. Libby,[16] A. Powell,[16] G. Wilkinson,[16] K. M. Ecklund,[17] W. Love,[18] V. Savinov,[18] A. Lopez,[19] H. Mendez,[19] J. Ramirez,[19] J. Y. Ge,[20] D. H. Miller,[20] I. P. J. Shipsey,[20] B. Xin,[20] G. S. Adams,[21] M. Anderson,[21] J. P. Cummings,[21] I. Danko,[21] D. Hu,[21] B. Moziak,[21] J. Napolitano,[21] Q. He,[22] J. Insler,[22] H. Muramatsu,[22] C. S. Park,[22] E. H. Thorndike,[22] and F. Yang[22]

(CLEO Collaboration)

[1]*Syracuse University, Syracuse, New York 13244, USA*
[2]*Wayne State University, Detroit, Michigan 48202, USA*
[3]*University of Bristol, Bristol BS8 1TL, United Kingdom*
[4]*Carleton University, Ottawa, Ontario, Canada K1S 5B6*
[5]*Carnegie Mellon University, Pittsburgh, Pennsylvania 15213, USA*
[6]*Enrico Fermi Institute, University of Chicago, Chicago, Illinois 60637, USA*
[7]*Cornell University, Ithaca, New York 14853, USA*
[8]*University of Florida, Gainesville, Florida 32611, USA*
[9]*George Mason University, Fairfax, Virginia 22030, USA*
[10]*University of Illinois, Urbana-Champaign, Illinois 61801, USA*
[11]*Indiana University, Bloomington, Indiana 47405, USA*
[12]*University of Kansas, Lawrence, Kansas 66045, USA*
[13]*Luther College, Decorah, Iowa 52101, USA*
[14]*University of Minnesota, Minneapolis, Minnesota 55455, USA*
[15]*Northwestern University, Evanston, Illinois 60208, USA*
[16]*University of Oxford, Oxford OX1 3RH, United Kingdom*
[17]*State University of New York at Buffalo, Buffalo, New York 14260, USA*
[18]*University of Pittsburgh, Pittsburgh, Pennsylvania 15260, USA*
[19]*University of Puerto Rico, Mayaguez, Puerto Rico 00681*
[20]*Purdue University, West Lafayette, Indiana 47907, USA*
[21]*Rensselaer Polytechnic Institute, Troy, New York 12180, USA*
[22]*University of Rochester, Rochester, New York 14627, USA*

Using 281 pb^{-1} of data collected with the CLEO-c detector, we present new measurements of Cabibbo-suppressed decays of D^0 and D^+ mesons to η and η' final states. We make first observations of $D^0 \to \eta' \pi^0$, $\eta\eta$, $\eta\eta'$, and $\eta\pi^+\pi^-$, and find evidence for $D^+ \to \eta\pi^+\pi^0$, $D^+ \to \eta'\pi^+\pi^0$, and $D^0 \to \eta'\pi^+\pi^-$. We also report on improved measurements of $D^0 \to \eta\pi^0$, $D^+ \to \eta\pi^+$, and $D^+ \to \eta'\pi^+$. Using the measured two-body Cabibbo-suppressed decays, we extract amplitudes for specific flavor topologies and compare them to those from Cabibbo-favored decays.

Charm decays provide a laboratory for the study of the weak and strong interactions. Because of their simplicity, two-body hadronic decays provide experimental input for understanding strong final state interaction effects in heavy meson decays [1–6]. By studying these decays, one can determine the magnitude and relative phases of contributing isospin or topological decay amplitudes. To describe these decays, particularly for *D* and *B* mesons, one often invokes symmetries, such as SU(3) flavor symmetry, which assumes the masses of the *u*, *d*, and *s* quarks are equal (and

implicitly assumed to be small). Small differences in decay rates are then attributed to SU(3) symmetry-breaking effects. Typically, such symmetry-breaking effects are at the level of 20% for D meson decays, and are expected to decrease as the parent meson mass increases, e.g., B decays. In the SU(3) flavor quark diagrammatic approach [4], two-body decays are decomposed into contributions from tree (T), color-suppressed (C), annihilation (A), and exchange (E) diagrams. Penguin diagrams are expected to be negligible in charm decays and are not discussed any further. Additional disconnected diagrams, such as the singlet-exchange (SE) and singlet-annihilation (SA) may also contribute to final states that include η and η' via their coupling to the SU(3) singlet component of these mesons. These quark diagrams are shown in Fig. 1.

An analysis of $D \rightarrow PP$ Cabibbo-favored (CF) decays has been carried out [7], and it was shown that their branching fractions are well-described within the SU(3) flavor topology approach. In this report, we measure branching fractions of singly Cabibbo-suppressed (CS) decays and analyze them within the same framework [8].

This analysis utilizes 281 pb^{-1} of data collected on the $\psi(3770)$ resonance at the Cornell Electron Storage Ring. This energy is just above threshold for production of $D\bar{D}$ pairs, and thus no additional particles accompany the pair. The decay products of the D mesons are reconstructed using the CLEO-c detector, which is a general purpose solenoidal detector. The detector includes a tracking system for measuring momenta and specific ionization (dE/dx) of charged particles, a Ring Imaging Cherenkov Counter (RICH) for particle identification, and a CsI calo-rimeter (CC) for detection of electromagnetic showers. The CLEO-c detector is described in detail elsewhere [9].

We reconstruct D meson candidates in the following singly Cabibbo-suppressed decay modes: $D^+ \rightarrow \eta\pi^+$, $\eta'\pi^+$, $\eta\pi^+\pi^0$, $\eta'\pi^+\pi^0$, and $D^0 \rightarrow \eta\pi^0$, $\eta'\pi^0$, $\eta\eta$, $\eta\eta'$, $\eta\pi^+\pi^-$, and $\eta'\pi^+\pi^-$. Unless otherwise noted, charge conjugate final states are assumed throughout.

Charged particles are reconstructed using the tracking system and are required to pass a set of standard selection criteria [10]. Charged pions are identified using a χ^2 discriminant based on dE/dx and RICH information. First, we require that the measured dE/dx is within 3 standard deviations (σ) of the expected value for a pion at the given momentum. We then define:

$$\Delta\chi^2 \equiv \chi_K^2 - \chi_\pi^2 + LL_K - LL_\pi, \qquad (1)$$

where $\chi_{K(\pi)}$ is the difference in the measured and expected dE/dx for the kaon (pion) hypothesis, normalized by its uncertainty, and $LL_{K(\pi)}$ is the negative log-likelihood for the kaon (pion) hypothesis obtained from the RICH. The RICH information is used only for charged particles with momentum above 0.7 GeV/c and possessing at least three associated Cherenkov photons. We require $\Delta\chi^2 > 0$, which results in an efficiency of about 95% and a fake rate of no more than 2%. We construct $\pi^0 \rightarrow \gamma\gamma$ and $\eta \rightarrow \gamma\gamma$ candidates using reconstructed showers in the calo-rimeter that have energy $E_\gamma > 30$ MeV ($E_\gamma > 50$ MeV for $\eta \rightarrow \gamma\gamma$) and no charged track that is projected within the vicinity of the shower. For each candidate, we require the mass pull, $\sigma_M \equiv (M_{\rm rec} - M_P)/\sigma_{M_{\rm rec}} < 3$, where $M_{\rm rec}$ is the reconstructed invariant mass, M_P is the parent particle mass (here π^0 or η), and $\sigma_{M_{\rm rec}}$ is the uncertainty in the invariant mass of the candidate ($\approx$ 5–7 MeV/c^2). Candidate $\eta \rightarrow \pi^+\pi^-\pi^0$ decays are also formed using the previously discussed selection criteria on charged and neutral pions. To improve the resolution on the π^0 or η momentum, the decays are kinematically constrained to the known π^0 and η meson masses. The improved four-momenta are then used in subsequent analysis. We select $\eta' \rightarrow \eta\pi^+\pi^-$ candidates by requiring the mass difference, $402 < M_{\eta\pi^+\pi^-} - M_\eta < 418$ MeV/c^2.

For D decay modes with only a single η, there is minimal benefit to including the $\eta \rightarrow \pi^+\pi^-\pi^0$ mode because of the lower branching fraction and detection efficiency. We therefore only use $\eta \rightarrow \gamma\gamma$. However, for $D^0 \rightarrow \eta\eta$ and $D^0 \rightarrow \eta\eta'$, there is a significant gain in statistical power by allowing one $\eta \rightarrow \pi^+\pi^-\pi^0$ decay in the final state. To reduce combinatoric background in three-body decays we veto $\eta \rightarrow \gamma\gamma$ candidates that share a photon with any π^0 with $|\sigma_M| < 3.0$. To ameliorate backgrounds from Cabibbo-favored modes containing a K_S^0 we require oppositely charged pion pairs in the final state to be outside the invariant mass interval from 475–520 MeV/c^2.
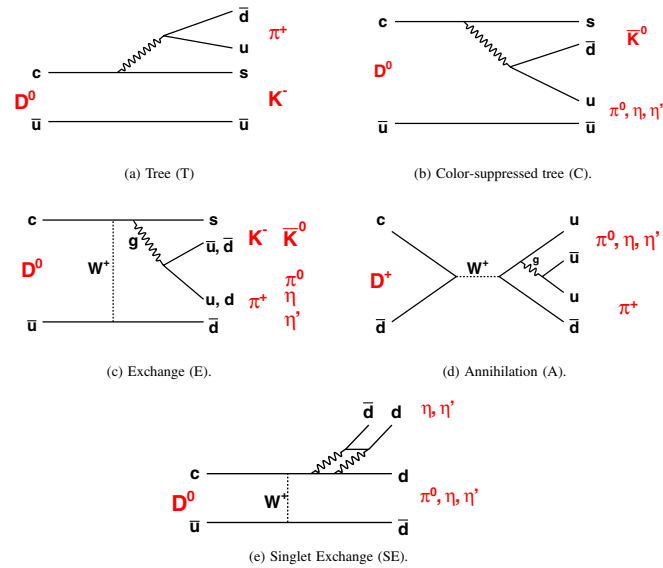

FIG. 1 (color online).   Feynman diagrams for various flavor topologies used to describe $D \rightarrow PP$ decays. Here, we use Cabibbo-favored diagrams as an example, for T, C, E, and Cabibbo-suppressed decays for the A and SE diagrams.

Signal *D* candidates are formed and required to have an energy, E_D, consistent with the beam energy, E_{beam}, by requiring $\Delta E \equiv E_D - E_{\text{beam}}$ is consistent with zero. The mode-by-mode ΔE selection requirements are determined from Monte Carlo simulation, and are shown in Table I. Efficiencies for these decays after all analysis requirements are determined from Monte Carlo simulation of these decays [11–13] and are also shown in Table I.

For candidates passing these selection criteria, we compute the beam-constrained mass, $M_{\text{bc}} = \sqrt{E_{\text{beam}}^2 - |\mathbf{p}_D|^2}$, where $\mathbf{p}_D$ is the momentum of the *D* candidate. Substituting E_{beam} for the candidate energy improves the mass resolution by about a factor of 2. Figure 2 shows the M_{bc} distributions for the two-body singly Cabibbo-suppressed decays (a) $D^+ \rightarrow \eta\pi^+$, (b) $D^0 \rightarrow \eta\pi^0$, (c) $D^+ \rightarrow \eta'\pi^+$, and (d) $D^0 \rightarrow \eta'\pi^0$, (e) $D^0 \rightarrow \eta\eta$, and (f) $D^0 \rightarrow \eta'\eta$. Prominent peaks are observed for all six decay modes. The points show the signal candidates in data and the curves are fits based on maximizing the likelihood of the probability density function, which is given by the sum of an ARGUS threshold function [14] and an asymmetric Gaussian signal shape (CBAL) [15]. The ARGUS shape parameters are extracted by fitting M_{bc} distributions obtained from the ΔE sideband regions in data. The high-mass tail in the M_{bc} spectrum results from initial state radiation (ISR) and is modeled by a power-law tail in the CBAL line-shape. The signal shape parameters (mean, width, and tail parameters) are determined from, and fixed to the values obtained from Monte Carlo simulation. We obtain yields of 1033 ± 42 for $D^+ \rightarrow \eta\pi^+$, 160 ± 24 for $D^0 \rightarrow \eta\pi^0$, 352 ± 20 for $D^+ \rightarrow \eta'\pi^+$, 50 ± 9 for $D^0 \rightarrow \eta'\pi^0$, 255 ± 22 for $D^0 \rightarrow \eta\eta$, and 46 ± 9 events for $D^0 \rightarrow \eta'\eta$. These are first observations of $D^0 \rightarrow \eta'\pi^0$, $D^0 \rightarrow \eta\eta$ and $D^0 \rightarrow \eta'\eta$, and correspond to signal significances of
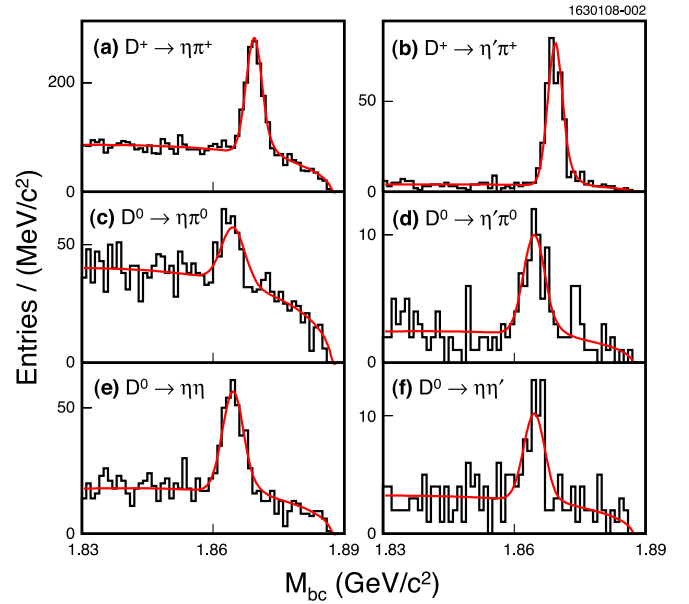

FIG. 2 (color online).   Distribution of M_{bc} for the two-body Cabibbo-suppressed decay modes: (a) $D^+ \rightarrow \eta\pi^+$, (b) $D^+ \rightarrow \eta'\pi^+$, (c) $D^0 \rightarrow \eta\pi^0$, (d) $D^0 \rightarrow \eta'\pi^0$, (e) $D^0 \rightarrow \eta\eta$, and (f) $D^0 \rightarrow \eta\eta'$. The superimposed curve is a fit to the data as described in the text.

7.2, 14.8, and 6.7, respectively. The significances are obtained from the differences in log-likelihood values with and without (signal yield set to zero) the signal component, i.e. $\sqrt{2\Delta \log L}$. The yields are shown in Table II. For $D^0 \rightarrow \eta\eta$ and $D^0 \rightarrow \eta\eta'$, we also show yields when the two η

TABLE I. Summary of mode-dependent ΔE selection requirements for modes under consideration. Also shown are the efficiencies from signal Monte Carlo simulation. For $D^0 \rightarrow \eta\eta$ and $D^0 \rightarrow \eta\eta'$, we indicate the decay modes of the η's in parentheses. The quoted uncertainties are statistical and systematic, respectively.

Mode	ΔE Range (MeV)	Efficiency (%)
$D^+ \rightarrow \eta\pi^+$	$[-28, 25]$	$46.7 \pm 0.5 \pm 1.7$
$D^+ \rightarrow \eta'\pi^+$	$[-19, 18]$	$27.7 \pm 0.5 \pm 1.1$
$D^0 \rightarrow \eta\pi^0$	$[-45, 34]$	$30.6 \pm 0.5 \pm 1.3$
$D^0 \rightarrow \eta'\pi^0$	$[-38, 32]$	$17.1 \pm 0.4 \pm 0.7$
$D^0 \rightarrow \eta\eta \ (\gamma\gamma)(\gamma\gamma)$	$[-33, 30]$	$28.9 \pm 0.4 \pm 2.2$
$D^0 \rightarrow \eta\eta(\gamma\gamma)(\pi^+\pi^-\pi^0)$	$[-26, 25]$	$16.5 \pm 0.4 \pm 0.7$
$D^0 \rightarrow \eta\eta' \ (\gamma\gamma)(\gamma\gamma)$	$[-27, 23]$	$15.9 \pm 0.4 \pm 1.2$
$D^0 \rightarrow \eta\eta'(\gamma\gamma)(\pi^+\pi^-\pi^0)$	$[-23, 20]$	$8.4 \pm 0.3 \pm 0.4$
$D^0 \rightarrow \eta\pi^+\pi^-$	$[-22, 19]$	$29.1 \pm 0.5 \pm 1.1$
$D^+ \rightarrow \eta\pi^+\pi^0$	$[-29, 24]$	$16.7 \pm 0.4 \pm 0.7$
$D^0 \rightarrow \eta'\pi^+\pi^-$	$[-19, 17]$	$13.3 \pm 0.3 \pm 0.5$
$D^+ \rightarrow \eta'\pi^+\pi^0$	$[-22, 20]$	$7.3 \pm 0.3 \pm 0.3$

TABLE II. Summary of yields and branching fraction measurements, as discussed in the text. For $D^0 \rightarrow \eta\eta$ and $D^0 \rightarrow \eta\eta'$, we also show the individual results obtained from the two η submodes. The first uncertainty is statistical and the second is systematic. Where measurements are available, results are compared to the PDG.

Mode	Yield	Branching Fraction (10^{-4})	PDG [16] (10^{-4})
$D^+ \rightarrow \eta\pi^+$	1033 ± 42	$34.3 \pm 1.4 \pm 1.7$	35.0 ± 3.2
$D^+ \rightarrow \eta'\pi^+$	352 ± 20	$44.2 \pm 2.5 \pm 2.9$	53 ± 11
$D^0 \rightarrow \eta\pi^0$	156 ± 24	$6.4 \pm 1.0 \pm 0.4$	5.6 ± 1.4
$D^0 \rightarrow \eta'\pi^0$	50 ± 9	$8.1 \pm 1.5 \pm 0.6$	—
$D^0 \rightarrow \eta\eta$	255 ± 22	$16.7 \pm 1.4 \pm 1.3$	—
$(\gamma\gamma)(\gamma\gamma)$	141 ± 17	15.3 ± 1.8 (stat.)	—
$(\gamma\gamma)(\pi^+\pi^-\pi^0)$	115 ± 13	19.0 ± 2.2 (stat.)	—
$D^0 \rightarrow \eta\eta'$	46 ± 9	$12.6 \pm 2.5 \pm 1.1$	—
$(\gamma\gamma)(\gamma\gamma)$	33 ± 8	14.8 ± 3.3 (stat.)	—
$(\gamma\gamma)(\pi^+\pi^-\pi^0)$	14 ± 5	10.5 ± 3.5 (stat.)	—
$D^0 \rightarrow \eta\pi^+\pi^-$	257 ± 32	$10.9 \pm 1.3 \pm 0.9$	<19
$D^+ \rightarrow \eta\pi^+\pi^0$	149 ± 34	$13.8 \pm 3.1 \pm 1.6$	—
$D^0 \rightarrow \eta'\pi^+\pi^-$	21 ± 8	$4.5 \pm 1.6 \pm 0.5$	—
$D^+ \rightarrow \eta'\pi^+\pi^0$	33 ± 9	$15.7 \pm 4.3 \pm 2.5$	—

decay channels are analyzed independently; both are consistent with fits to the sum of both decay channels.

Peaking backgrounds from nonresonant final states, such as $D^0 \to \eta\pi^+\pi^-\pi^0$, $D^0 \to \eta\eta\pi^+\pi^-$, etc., which may contribute to the $D^0 \to \eta\eta$ and $D^0 \to \eta\eta'$ decays, respectively, are highly suppressed because the $\pi^+\pi^-\pi^0$ and $\eta\pi^+\pi^-$ invariant masses must be consistent with the η and η' masses, respectively. Moreover, these backgrounds are also Cabibbo suppressed, and thus we expect them to be very small or negligible. This supposition is checked by selecting candidates from the sideband regions, $7 < |\sigma_M| < 10$ and $8 < M_{\pi^+\pi^-\eta} - M_\eta - 410 < 16 \,\mathrm{MeV}/c^2$, and repeating the analysis. No evidence of peaking backgrounds are found.

Figure 3 shows the M_{bc} distributions for the three-body Cabibbo-suppressed decays. (a) $D^0 \to \eta\pi^+\pi^-$, (b) $D^+ \to \eta\pi^+\pi^0$, (c) $D^0 \to \eta'\pi^+\pi^-$, and (d) $D^+ \to \eta'\pi^+\pi^0$. We obtain signal yields (significances) of 258 ± 32 (9.0) for $D^0 \to \eta\pi^+\pi^-$, 147 ± 34 (4.5) for $D^+ \to \eta\pi^+\pi^0$, 21 ± 8 (3.2) for $D^0 \to \eta'\pi^+\pi^-$, and 33 ± 9 (4.2) for $D^+ \to \eta'\pi^+\pi^0$, respectively. We thus establish the $D^0 \to \eta\pi^+\pi^-$ decay, and provide first evidence for the other three-body decay modes.

The branching fractions are computed from:

$$\mathcal{B} = \frac{N_{\mathrm{sig}}}{2N_{D\bar{D}}A}, \qquad (2)$$

where N_{sig} is the number of signal events, $N_{D\bar{D}}$ is the number of $D\bar{D}$ pairs produced, and the acceptance $A = \sum \epsilon_i \mathcal{B}_\eta^i$. Here, the sum is over the product of efficiency (ϵ_i) and $\eta^{(')}$ submode branching fractions, for the measurements indicated in Table II. The numbers, $N_{D^0\bar{D}^0} = (1.031 \pm 0.015) \times 10^6$ and $N_{D^+D^-} = (0.819 \pm 0.013) \times 10^6$, are determined from an independent measurement of Cabibbo-favored D hadronic branching fractions [10]. The yields and branching fractions are tabulated in Table II. For $D^0 \to \eta\eta$ and $D^0 \to \eta\eta'$ we also show that the two decay modes yield consistent branching fractions.

The inclusive rates for $D \to \eta^{(')}X$ have been recently measured [17], and the exclusive $D^0 \to \eta X$, $D^0 \to \eta'X$ and $D^+ \to \eta X$ modes measured here comprise about 10% of their respective total inclusive rates. In contrast, $\mathcal{B}(D^+ \to \eta'\pi^+) + \mathcal{B}(D^+ \to \eta'\pi^+\pi^0) \simeq 0.6\%$ accounts for about 60% of the total inclusive rate.

A number of systematic uncertainties have been considered. Efficiencies, as determined from Monte Carlo simulation, are subject to uncertainties due to finite statistics (1%–2%), modeling of the underlying physics, and modeling of the detector response. The underlying physics that induces uncertainty in the efficiencies includes modeling of final state radiation (1%) and resonant substructure. The latter is applicable only to the three-body decay modes and is determined by comparing efficiencies determined using a phase-space decay with those obtained using intermediate resonances, such as $\eta^{(')}\rho$, $a_0(980)\pi$, or $a_0(1450)\pi$. We take the largest fractional difference in efficiency as the associated uncertainty. The values range from 3% for $D^0 \to \eta\pi^+\pi^-$ to 12% for $D^+ \to \eta'\pi^+\pi^0$. Charged and neutral particle reconstruction and identification has been extensively studied using a missing-mass technique [10], and we find that the efficiencies in data are consistent with, or slightly lower than simulated efficiencies. We thus correct the simulated efficiencies as follows. The pion tracking efficiency and particle identification corrections are 1.000 ± 0.003 and 0.9950 ± 0.0025, respectively. For each $\pi^0 \to \gamma\gamma$ ($\eta \to \gamma\gamma$), we adjust the efficiencies by 0.961 ± 0.020 (0.943 ± 0.035). These corrections and uncertainties are included in the efficiencies shown in Table I.

Additional sources of uncertainty arise from the candidate selection requirements, namely, the K_S^0 veto, η' mass window, $\eta \to \gamma\gamma$ veto (for photons also used in a π^0), and the restricted ΔE range. We estimate the uncertainty introduced from these requirements by increasing the window size and taking the fractional difference in the efficiency-corrected yield between the nominal and the larger window size. For the K_S^0 rejection, we increase the veto region by $\pm 50\%$, from which we find an uncertainty of 2%. For the η' selection, we broaden the selection window to cover the range from 395–423 MeV/c^2, and find an associated uncertainty of 1%. The uncertainty introduced from the $\eta \to \gamma\gamma$ veto is only applicable to three-body decay modes. It is estimated by comparing (data and MC simulation) the fraction of signal events
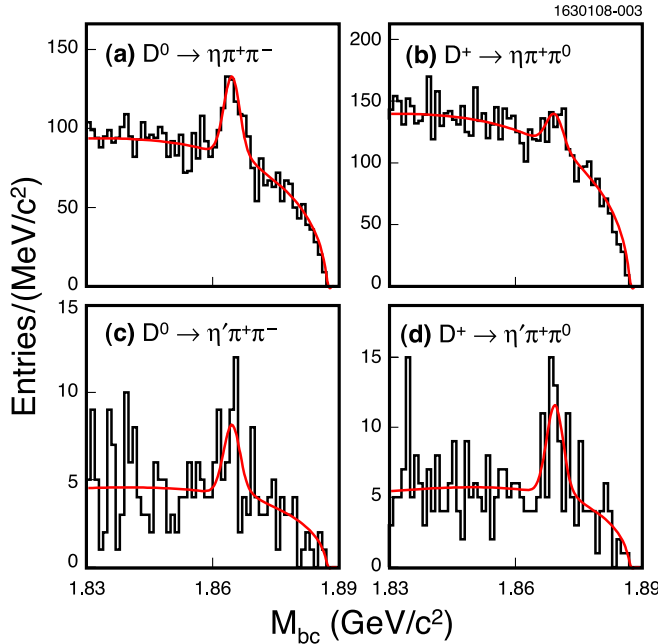

FIG. 3 (color online). Distribution of M_{bc} for the three-body Cabibbo-suppressed decay modes: (a) $D^0 \to \eta\pi^+\pi^-$, (b) $D^+ \to \eta\pi^+\pi^0$, (c) $D^0 \to \eta'\pi^+\pi^-$, and (d) $D^+ \to \eta'\pi^+\pi^0$. The superimposed curve is a fit to the data as described in the text.

that pass the veto with respect to no veto in the two-body decay modes. The ratio, averaged over several modes, is 1.01 ± 0.02, and we conservatively assign a 5% systematic error to this source. The ΔE systematic uncertainty is obtained by increasing the ΔE signal window by one unit of the Gaussian width. The corresponding uncertainty ranges from 2% for $D^+ \to \eta \pi^+$ to 4% for $D^0 \to \eta \pi^0$. Uncertainty in the signal yield receives contributions from both the signal and background shape parametrizations. Both are studied by varying the shape parameters one at a time by ± 1 standard deviation and adding the resulting changes in yield in quadrature. The associated uncertainties range from 1% (for $D \to \eta \pi^+$) to 4% (for $D^0 \to \eta' \pi^+ \pi^-$) for the signal shape uncertainty and 0.5% (for $D \to \eta' \pi^+$) to 4.0% (for $D^0 \to \eta' \pi^+ \pi^-$) for the background shape and normalization. Uncertainty due to multiple candidates in an event is quantified by computing the average number of candidates per event within ± 5 MeV of the known D mass for both simulation and data. We find good agreement between data and simulation, except for final states with low momentum π^0's, where the data has a slightly larger rate of multiple candidates. We take half the difference between the average number of multiple candidates between data and simulation as a correction to the branching fraction, and assign 100% uncertainty to it, leading to the following corrections: 1.013 ± 0.013 for $D^+ \to \eta \pi^+ \pi^0$, 1.015 ± 0.015 for $D^+ \to \eta' \pi^+ \pi^0$, and 1.03 ± 0.03 for $D^0 \to (\eta \to \gamma\gamma)(\eta \to \pi^+ \pi^- \pi^0)$. The rest of the modes are consistent with unity at the level of 1%, which we assign as a systematic uncertainty. The branching fractions for $\eta \to \gamma\gamma$, $\eta \to \pi^+ \pi^- \pi^0$, and $\eta' \to \eta \pi^+ \pi^-$ are uncertain by 0.6%, 1.5%, and 3.1%, respectively, for each such decay in the final state. Lastly, the number of $D^0 \bar{D}^0$ ($D^+ D^-$) events in our data sample has an uncertainty of 1.5% (1.6%) [10]. The systematic uncertainties for all modes under consideration are summarized

in Tables III and are included in the branching fraction measurements in Table II.

We have searched for intermediate resonances in $D^0 \to \eta \pi^+ \pi^-$. Figure 4 shows the sideband-subtracted $\eta \pi^+$ and $\pi^+ \pi^-$ invariant mass distributions. Surprisingly, there are no significant contributions from either $\eta \rho^0$ or $a_0(980)\pi^+$. Overlayed on the data (points) is a Monte Carlo simulation where a phase-space model is used. We find that decay is well-modeled by three-body phase space.

We now apply a SU(3) diagrammatic analysis to test the validity of the SU(3) flavor decomposition approach to charm meson decays [4,7,8]. Two-body D meson decays can be described using a SU(3) diagrammatic approach in terms of an external tree diagram, T; a color-suppressed tree diagram, C; an exchange diagram, E; an annihilation diagram, A; and a singlet-exchange diagram, SE. The SE contribution represents the matrix element that produces an η or η' through its coupling to the SU(3) singlet portion of these mesons. Such contributions are OZI-suppressed, and thus expected to be small. These five diagrams are shown in Fig. 1.

We first update the fitted diagrammatic amplitudes obtained from Cabibbo-favored decays [8]. Table IV shows the SU(3) representations, the measured branching fractions, decay momentum (p^*), and invariant amplitudes for Cabibbo-favored $D \to PP$ decays. The lifetime of the D mesons and the $D \to \bar{K}^0(\eta, \eta')$ branching fractions are taken from the PDG [16], whereas the other six branching fractions are taken from recent CLEO measurements [10,18,19]. The eight branching fraction measurements are fit to four topological amplitudes and three relative strong phases. The phases of C, E, and A are measured with respect to T, which is taken to be real. The phase, δ_{AB} is the angle subtended from amplitude B to amplitude A. The fitted amplitudes (in units of 10^{-6} GeV) and relative strong phases are found to be:

TABLE III. Systematic uncertainties for signal D decay modes as discussed in the text. The two entries for $D^0 \to \eta\eta$ and $D^0 \to \eta\eta'$ correspond to the final states that are reconstructed with two $\eta \to \gamma\gamma$ decays, or one $\eta \to \gamma\gamma$ and one $\eta \to \pi^+ \pi^- \pi^0$.

| Source	$\eta\pi^+$	$\eta'\pi^+$	$\eta\pi^0$	$\eta'\pi^0$	$\eta\eta$	$\eta\eta'$	$\eta\pi^+\pi^0$	$\eta'\pi^+\pi^0$	$\eta\pi^+\pi^-$	$\eta'\pi^+\pi^-$
MC Statistics	1.0	1.0	1.0	1.0	1.0	1.0	2.0	2.0	1.0	2.0
Particle Recon. & ID	3.7	3.9	4.3	4.3	7.4/4.3	7.5/4.5	4.3	4.4	3.8	4.0
ΔE Selection	2.0	2.0	4.0	3.0	3.0/2.0	2.0/2.0	4.0	3.0	3.0	2.0
η' Selection	—	1.0	—	1.0	—	1.0	—	1.0	—	1.0
Signal Shape	1.0	3.0	1.0	3.0	3.0	2.0	2.0	3.0	3.0	4.0
Background	0.6	0.5	2.7	3.2	1.4	3.1	1.6	4.4	2.7	3.2
Multiple Candidates	1.0	1.0	1.0	1.0	1.0/3.0	1.0/1.0	1.3	1.5	1.0	1.0
$\eta \to \gamma\gamma$ Veto	—	—	—	—	—	—	5.0	5.0	5.0	5.0
Resonant Substructure	—	—	—	—	—	—	8.0	12.0	3.0	5.0
Final State Rad.	1.0	1.0	1.0	1.0	1.0	1.0	1.0	1.0	1.0	1.0
K_S^0 Veto	—	—	—	—	—	—	—	—	2.0	2.0
$N_{D\bar{D}}$	1.6	1.6	1.5	1.5	1.5	1.5	1.6	1.6	1.5	1.5
$\mathcal{B}_{(\eta')}$	0.6	3.2	0.6	3.2	1.2/2.1	3.4/3.6	0.6	3.2	0.6	3.2
Total	4.9	6.1	6.9	7.6	7.7	8.6	11.8	15.7	8.6	11.4
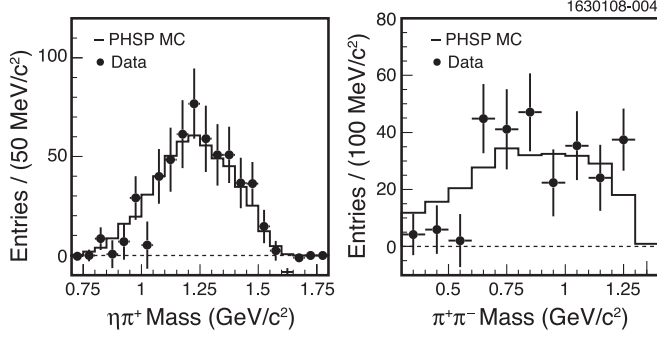
FIG. 4. Sideband-subtracted invariant mass distributions for $\eta\pi^+$ (left) and $\pi^+\pi^-$ (right) in the $D^0 \to \eta\pi^+\pi^-$ decay. The points are data and the histogram is a phase space (PHSP) model of the decay from Monte Carlo simulation.

$$T = (2.78 \pm 0.13), \tag{3a}$$

$$C = (2.04 \pm 0.17)e^{i(-151\pm2)^\circ}, \tag{3b}$$

$$E = (1.68 \pm 0.12)e^{i(117\pm4)^\circ}, \tag{3c}$$

$$A = (0.54 \pm 0.37)e^{i(-64^{+32}_{-8})^\circ}. \tag{3d}$$

The fit χ^2 is 0.65 for 1 degree of freedom, indicating that the OZI-suppressed SE and SA contributions are not needed to describe the branching fraction measurements in Cabibbo-favored decays. These results are consistent

TABLE VI. Solutions for the topological amplitudes using Cabibbo-suppressed decays. The fit results are compared to the values from Cabibbo-favored decays, scaled by $\lambda \equiv \tan\theta_C = 0.2317$.

Amplitude	Magnitude $(10^{-7}$ GeV)		δ_{CE} (°)	
	CS	$\lambda \times$ CF	CS	CF
C	5.8 ± 0.3	4.7 ± 0.4	—	—
E	3.5 ± 0.3	3.9 ± 0.3	77 ± 7	92 ± 4

with those obtained in Ref. [8] and the fitted branching fractions ($\mathcal{B}_{\text{fit}}$ in Table IV) are in good agreement with the experimental values.

We now analyze the Cabibbo-suppressed decays using the same framework. Using our measured branching fractions for $D^0 \to \eta\pi^0$, $D^0 \to \eta'\pi^0$, $D^0 \to \eta\eta$, and $D^0 \to \eta\eta'$, we extract C' and E', the analog of C and E for CS decays. The topological amplitudes for these decays are given in Table V. We first assume $SE' = 0$ and using these four measured branching fractions, we fit for C', E', and $\cos\delta_{C'E'}$. The resulting amplitudes and relative strong phase are shown in Table VI, and are compared to the values from CF decays, scaled by $\lambda \equiv \tan\theta_C = 0.2317$ [16]. The values agree within about 2 standard deviations, and are well within the oft cited $\sim$20% level of SU(3) symmetry-breaking effects in D meson decays.

TABLE IV. Table of branching fractions, SU(3) representations [8], decay momenta, and invariant amplitudes for $D \to PP$ Cabibbo-favored decays. The last column shows the fitted branching fractions as described in the text. The branching fractions, $\mathcal{B}_{\text{exp}}$, are taken from recent CLEO measurements [10,18,19] when available, otherwise we use PDG values [16].

Mode	Representation	$\mathcal{B}_{\text{exp}}$ (%)	p^* (MeV)	$\mathcal{A}$ $(10^{-6}$ GeV)	$\mathcal{B}_{\text{fit}}$ (%)
$D^0 \to K^-\pi^+$	$T + E$	3.891 ± 0.077	861	2.52 ± 0.02	3.899
$D^0 \to \bar{K}^0\pi^0$	$\frac{1}{\sqrt{2}}(C - E)$	2.238 ± 0.109	860	1.91 ± 0.05	2.208
$D^0 \to \bar{K}^0\eta$	$\frac{1}{\sqrt{3}}C$	0.76 ± 0.11	772	1.18 ± 0.09	0.76
$D^0 \to \bar{K}^0\eta'$	$\frac{-1}{\sqrt{6}}(C + 3E)$	1.87 ± 0.28	565	2.16 ± 0.16	1.95
$D^+ \to \bar{K}^0\pi^+$	$(C + T)$	2.986 ± 0.067	862	1.39 ± 0.02	2.99
$D_s^+ \to \bar{K}^0 K^+$	$(C + A)$	2.98 ± 0.17	850	2.12 ± 0.06	3.02
$D_s^+ \to \eta\pi^+$	$\frac{1}{\sqrt{3}}(T - 2A)$	1.58 ± 0.21	902	1.50 ± 0.10	1.47
$D_s^+ \to \eta'\pi^+$	$\frac{2}{\sqrt{6}}(T + A)$	3.77 ± 0.39	743	2.55 ± 0.13	3.61

TABLE V. SU(3) representations [8], measured branching fractions (from this analysis), decay momenta, and invariant amplitudes for selected Cabibbo-suppressed decays. The branching fraction uncertainties are obtained from the quadrature sum of the statistical and systematic uncertainties.

Mode	Representation $(SE' = 0)$	Representation $(SE' \neq 0)$	$\mathcal{B}_{\text{exp}}$ (10^{-4})	p^* (MeV)	$\mathcal{A}$ $(10^{-7}$ GeV)
$D^0 \to \eta\pi^0$	$\frac{1}{\sqrt{6}}(C' - 2E')$	$\frac{1}{\sqrt{6}}(C' - 2E' - SE')$	6.4 ± 1.1	846	3.26 ± 0.28
$D^0 \to \eta'\pi^0$	$\frac{1}{\sqrt{3}}(C' + E')$	$\frac{1}{\sqrt{3}}(C' + E' + 2SE')$	8.1 ± 1.6	678	4.09 ± 0.40
$D^0 \to \eta\eta$	$\frac{2\sqrt{2}}{3}C'$	$\frac{2\sqrt{2}}{3}(C' + SE')$	16.7 ± 1.9	755	5.57 ± 0.32
$D^0 \to \eta\eta'$	$\frac{-1}{3\sqrt{2}}(C' + 6E')$	$\frac{-1}{3\sqrt{2}}(C' + 6E' + 7SE')$	12.6 ± 2.7	537	5.74 ± 0.61

We now allow for an additional singlet-exchange amplitude, SE' [8]. The SU(3) representations, including SE', are shown in Table V. Invoking SU(3) symmetry, we have $T' = \lambda T$, $C' = \lambda C$, $E' = \lambda E$ and $A' = \lambda A$, $\delta_{C'T'} = \delta_{CT}$, $\delta_{E'T'} = \delta_{ET}$, and $\delta_{A'T'} = \delta_{AT}$. The amplitudes T', C', E', and A' (in units of 10^{-7} GeV) are found to be:

$$T' = 6.44 \pm 0.30, \tag{4a}$$

$$C' = 4.73 \pm 0.39 e^{i(-151\pm2)°}$$
$$= (-4.15 \pm 0.38) + i(-2.25 \pm 0.15), \tag{4b}$$

$$E' = 3.89 \pm 0.28 e^{i(-117\pm4)°}$$
$$= (-1.76 \pm 0.24) + i(3.48 \pm 0.29), \tag{4c}$$

$$A' = 1.25 \pm 0.86 e^{i(-64^{+32}_{-8})°}$$
$$= (0.55 \pm 0.34) + i(-1.14 \pm 0.83). \tag{4d}$$

One may rewrite the amplitudes in Table V as follows [8]:

$$-\sqrt{6}\mathcal{A}(D^0 \to \eta\pi^0) = 2E' - C' + SE'$$
$$= (0.63 + i9.21) \times 10^{-7} \text{ GeV} + SE', \tag{5a}$$

$$\frac{\sqrt{3}}{2}\mathcal{A}(D^0 \to \eta'\pi^0) = \frac{1}{2}(C' + E') + SE'$$
$$= (-2.95 + i0.61) \times 10^{-7} \text{ GeV} + SE' \tag{5b}$$

$$\frac{3}{2\sqrt{2}}\mathcal{A}(D^0 \to \eta\eta) = C' + SE'$$
$$= (-4.15 - i2.25) \times 10^{-7} \text{ GeV} + SE' \tag{5c}$$

$$\frac{-3\sqrt{2}}{7}\mathcal{A}(D^0 \to \eta\eta') = \frac{1}{7}(C' + 6E') + SE'$$
$$= (-2.10 + i2.66) \times 10^{-7} \text{ GeV} + SE' \tag{5d}$$

The right-hand side of each of these four equations defines a vector in the complex plane, which contains an unknown complex offset, SE'. The left-hand side of these equations defines four circles in the complex plane, whose radii are determined by their measured branching fractions. We thus have four constraints with which to solve for the real and imaginary parts of SE'. The solutions are obtained graphically from the common intersection point(s) of these four circles.

Figure 5 shows Eqs. (5a)–(5d) graphically, where we find two common intersection points, which are (the negative of) the allowed SE' solutions. The small solution $\text{Re}(SE') = (-0.7 \pm 0.4) \times 10^{-7}$ GeV and $\text{Im}(SE') = (-1.0 \pm 0.6) \times 10^{-7}$ GeV, is favored due to the expected OZI suppression. The larger solution, which is disfavored,
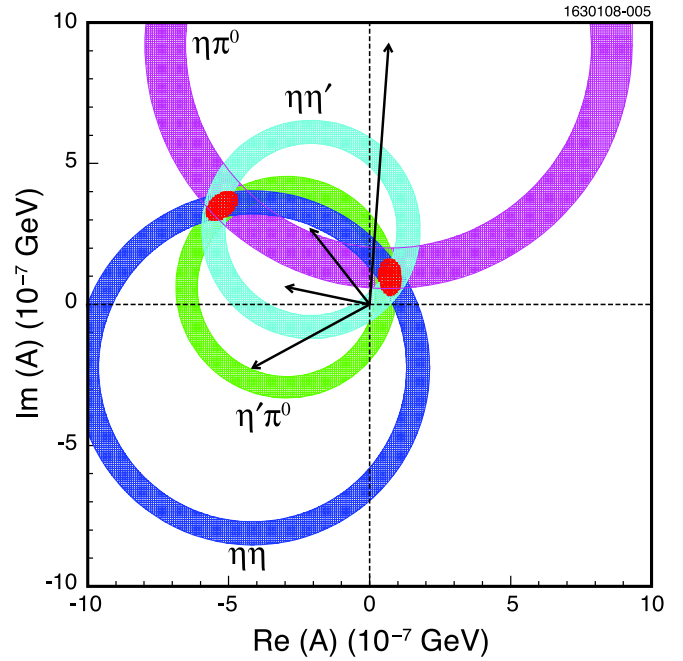

FIG. 5 (color online). Graphical presentation of the four Cabibbo-suppressed amplitudes as circles in the complex plane. The arrows correspond to their centers, as determined from Cabibbo-favored decays, scaled by $\tan\theta_C = 0.2317$. The two overlap regions correspond to the allowed SE' solutions.

corresponds to $\text{Re}(SE') = (5.3 \pm 0.5) \times 10^{-7}$ GeV and $\text{Im}(SE') = (-3.5 \pm 0.5) \times 10^{-7}$ GeV. We thus find that apart from a small additional SE' contribution to CS decays, $C' \simeq \lambda C$ and $E' \simeq \lambda E$, and thus these decays respect SU(3) symmetry at the level of $\sim 20\%$. We therefore find that this SU(3) flavor diagrammatic approach provides a reasonable description of both Cabibbo-favored and Cabibbo-suppressed $D \to PP$ decays that depend on C and E diagrams. This SU(3) topological approach may not apply equally well to all decays. For example, it is well known that the prediction $\mathcal{B}(D^0 \to \pi^+\pi^-) = \mathcal{B}(D^0 \to K^+K^-)$ is not realized due to SU(3) symmetry-breaking effects in the form factors and decays constants.

In summary we report on first observations of $D^0 \to \eta'\pi^0$, $D^0 \to \eta\eta$, $D^0 \to \eta\eta'$, and $D^0 \to \eta\pi^+\pi^-$. We also find evidence for the three-body decays $D^+ \to \eta\pi^+\pi^0$, $D^0 \to \eta'\pi^+\pi^-$, and $D^+ \to \eta'\pi^+\pi^0$. We have analyzed $D^0 \to \eta\pi^0$, $\eta'\pi^0$, $\eta\eta$ and $D^0 \to \eta\eta'$ decays within the SU(3) flavor topology approach [8] and find that the color-suppressed and exchange amplitudes have magnitudes and a relative strong phase that are consistent with Cabibbo-favored decays. We have performed a second fit where we allow for an additional singlet-exchange amplitude and find a solution near zero (favored) and a larger solution, which is disfavored due to the OZI suppression of this process.

---

[1] J. H. Lai and K. C. Yang, Phys. Rev. D **72**, 096001 (2005).

[2] P. Guo, X.-G. He, and X.-Q. Li, Int. J. Mod. Phys. A **21**, 57 (2006).

[3] M. Ablikim, D.-S. Du, and M.-Z. Yang, High Energy Phys. Nucl. Phys. **27**, 759 (2003); Phys. Lett. B **536**, 34 (2002).

[4] J. L. Rosner, Phys. Rev. D **60**, 074029 (1999), and references therein.

[5] F. Buccella, M. Lusignoli, and A. Pugliese, Phys. Lett. B **379**, 249 (1996).

[6] A. N. Kamal, Int. J. Mod. Phys. A **7**, 3515 (1992).

[7] J. L. Rosner, Phys. Rev. D **60**, 114026 (1999).

[8] C.-W. Chiang, Z. Luo, and J. L. Rosner, Phys. Rev. D **67**, 104001 (2003).

[9] D. Peterson *et al.*, Nucl. Instrum. Methods Phys. Res., Sect. A **478**, 142 (2002); M. Artuso *et al.*, Nucl. Instrum. Methods Phys. Res., Sect. A **554**, 147 (2005); Y. Kubota *et al.*, Nucl. Instrum. Methods Phys. Res., Sect. A **320**, 66 (1992).

[10] S. Dobbs *et al.* (CLEO Collaboration), Phys. Rev. D **76**, 112001 (2007); Q. He *et al.* (CLEO Collaboration), Phys. Rev. Lett. **95**, 121801 (2005).

[11] D. J. Lange, Nucl. Instrum. Methods Phys. Res., Sect. A **462**, 152 (2001).

[12] R. Brun *et al.*, GEANT 3.21, CERN Program Library Long Writeup W5013, 1993 (unpublished).

[13] E. Barberio and Z. Was, Comput. Phys. Commun. **79**, 291 (1994).

[14] H. Albrecht *et al.* (ARGUS Collaboration), Phys. Lett. B **229**, 304 (1989).

[15] T. Skwarnicki, Ph.D. thesis, DESY [Report No. F31-86-02, 1986 (unpublished)].

[16] W.-M. Yao *et al.*, J. Phys. G **33**, 1 (2006).

[17] G. S. Huang *et al.* (CLEO Collaboration), Phys. Rev. D **74**, 112005 (2006).

[18] J. P. Alexander *et al.* (CLEO Collaboration), Phys. Rev. Lett. **100**, 161804 (2008).

[19] Q. He *et al.* (CLEO Collaboration), arXiv:0711.146.